

PARALLELPROJ - An open-source framework for fast calculation of projections in tomography

Georg Schramm^{1,2}

¹Radiological Sciences Lab, Stanford School of Medicine, Stanford University, Stanford, US

²Department of Imaging and Pathology, Division of Nuclear Medicine, KU Leuven, Belgium

Abstract: In this article, we present a new open source framework, called `parallelproj`, for fast parallel calculation of projections in tomography using multiple CPUs or GPUs. This framework implements forward and back projection functions in sinogram and listmode using Joseph’s method, which is also extended for time-of-flight PET projections. In a series of tests related to PET image reconstruction using data from a state-of-the-art clinical PET/CT system, we benchmark the performance of the projectors in non-TOF and TOF, sinogram and listmode using a multi CPU, hybrid CPU/GPU and pure GPU mode. We find that the GPU mode offers acceleration factors between 20 and 60 compared to the multi CPU mode and that OSEM listmode reconstruction of real world PET data sets is possible within a couple of seconds using a single state-of-the-art GPU.

1 Introduction

For tomographic imaging techniques used in medicine such as X-ray computed tomography (CT), positron emission tomography (PET) and single photon emission tomography (SPECT), image reconstruction results are usually expected within seconds or minutes after data acquisition, creating a severe computational challenge when reconstruction data from state-of-the-art systems. With new scanner generations, the problem size of this challenge is steadily growing, since (i) the data size is increasing due to higher resolution detectors and scanners with bigger field of view [1], and (ii) more advanced (iterative) reconstruction algorithms are being used that try to exploit more information from the acquired data, which usually necessitates the calculation of a huge amount of projections. An example of the latter is the data-driven motion correction in PET [2] where instead of reconstructing a single “static frame”, many very short time frames are reconstructed and subsequently used for motion estimation and correction. Another example for (ii) is the combination of deep learning and tomographic image reconstruction [3]–[5], using, e.g. unrolled networks, where during training also a tremendous number of projections have to be calculated to evaluate the gradient of the data fidelity term across a mini batch in every training epoch.

For most tomographic image reconstruction algorithms, the bottleneck in terms of computation time is the evaluation of a linear forward model that describes the physics of the data acquisition process. In CT, PET, and SPECT, the forward model includes the computation of many (weighted) line or volume integrals through an image volume, commonly called “projections” - which can be slow when executed on a single processor. Fortunately, for most reconstruction algorithms, the computation of projections can be executed in parallel on multiple processors, e.g. using multiple CPUs or one or more graphics processing units (GPUs). Note that the

evaluation of the adjoint of the forward model - commonly called “back projection” - is computationally more demanding, since race conditions usually occur. In recent decades, the use of GPUs for faster calculation of projections in tomographic imaging has been studied extensively; see, e.g. [6]–[21] or the reviews [22], [23] for the use of GPUs in PET reconstruction. All of these articles conclude that the time needed to calculate forward and back projections on state-of-the-art GPUs is usually much shorter compared to using multiple CPUs. Motivated by these findings and the recent availability of very powerful low- and high-level GPU programming frameworks such as CUDA and cupy [24], we developed a new open source research framework, called `parallelproj`, for fast calculations of projections in tomography.

The objectives of the `parallelproj` framework are as follows:

- To provide an open source framework for fast parallel calculation of projections in tomographic imaging using multiple CPUs or GPUs.
- To provide an accessible framework that can be easily installed without the need for compilation of source code on all major operating systems (Linux, Windows, and macOS).
- To provide a framework that can be efficiently used in conjunction with `pytorch` [25] GPU arrays to facilitate research on tomographic imaging methods, including deep learning.

This article on the `parallelproj` framework is organized as follows. We first review Joseph’s method for calculating projections, followed by a short overview of the design choices and implementation of `parallelproj`. Subsequently, we report the results of a few benchmarks related to image reconstruction in PET with and without time-of-flight (TOF) information

using sinograms or listmode (LM) before ending the article with a detailed discussion and conclusion. In this article, we focus on the performance of `parallelproj` projectors for non-TOF and TOF PET reconstruction problems. Note, however, that the non-TOF Joseph projectors could also be used in iterative CT or SPECT reconstruction.

2 Materials and Methods

2.1 Joseph’s method for projecting rays through voxel images

Besides Siddon’s method [26] and the distance-drive method [27], Joseph’s method [28] is a very efficient and popular way to calculate projections in transmission and emission tomography. The basic idea of the original Joseph method for calculating line integrals, that can be used to model non-TOF projections, is shown in Figure 1. For a given ray, the algorithm first determines the principal direction that is most parallel to the ray and then steps through the image volume plane by plane along this principal direction. In every plane, the intersection point between the ray and the plane is calculated and the contribution of the image at that point to the line integral is approximated using bi-linear of the four nearest neighbors around the intersection point. In other words, only the four nearest neighboring voxels are contributing to the line integral and their contributions are given by the bi-linear interpolation weights. Finally, the contributions of all planes are added and corrected for the incidence angle of the ray - see [28] for more details. An extension of the original Joseph method to calculate TOF-weighted projections is straight forward. For every voxel contributing to the line integral and every TOF bin along the ray, a TOF weight can be computed by evaluating a TOF kernel that is a function of the Euclidean distance between the voxel and the center of the TOF bin. The TOF kernel can be, e.g. modeled as a Gaussian kernel convolved with the width of the TOF bins, resulting in the evaluation of the difference of two error functions.

2.2 Design principles and implementation details

The application programming interface to the `parallelproj` framework was designed such that:

- The input to the low level projector functions are as generic as possible. In practice, that means that these functions take a list of coordinates representing the start and end point of the rays to be projected as input, making the low-level functions agnostic to specific scanner geometries (or symmetries). Thus, any scanner geometry can be modeled.
- Projections can be performed in non-TOF or TOF mode.

- In the TOF mode, optimized projections for sinogram and listmode are available. In the former, the contributions to all available TOF bins along a ray are computed while traversing the image volume plane by plane, whereas in the latter only the contribution to one specific TOF bin (the TOF bin of a given listmode event) is evaluated.
- The back projections are the exact adjoint of the forward projections (matched forward and back projections).

Parallelization across multiple processors was implemented in two different ways. To enable parallelization across multiple CPUs, a first version of the `parallelproj` library was implemented using C and OpenMP [29] (`libparallelproj_c`). Furthermore, the exact same projector functions were implemented in CUDA to enable parallelization on one or multiple GPUs (`libparallelproj_cuda`). In the CUDA version, the input data is first transferred from the host to all available GPU(s) followed by the parallel execution of the projection kernels. After the kernel execution, the result is transferred back to the host. To handle race conditions, all implementations use atomic add operations in the back projections.

2.3 Availability of source code and precompiled libraries

`parallelproj` is an open source project and the source code is available at <https://github.com/gschramm/parallelproj> under MIT license. Next to the sources, we also offer precompiled libraries for all major operating systems (Linux, Windows, and macOS) and various recent CUDA versions using the `conda-forge` package manager.¹ In addition to the precompiled libraries, the `parallelproj` package also includes the source file of the CUDA projection kernels such that they can be directly executed on GPU arrays using frameworks that allow for just-in-time compilation of CUDA kernels such as, e.g. `cupy` [24].

2.4 parallelproj computation modes

Using the two aforementioned projection libraries, as well as the CUDA projections kernels, projections can be performed in the following three different computation modes:

1. **CPU mode:** Forward and back projections of image volumes (arrays) stored on the host (CPU) can be performed using `libparallelproj_c` where parallelization across all available CPUs is performed using OpenMP.
2. **hybrid CPU/GPU mode:** Forward and back projections of image volumes (arrays) stored on the host can be performed using `libparallelproj_cuda` involving data transfer from the host to all available GPUs, execution

¹The CUDA version of the `parallelproj` library is not available for macOS.

of projection kernels on the GPUs, and transfer of the results back to the host.

3. **direct GPU mode:** Forward and back projections of image volumes (arrays) stored on a GPU can be performed by direct execution of the projection kernels using a framework that supports just-in-time compilation of CUDA kernels, such as cupy [24]. In contrast to the hybrid CPU/GPU mode, memory transfer between host and GPU is avoided.

2.5 Benchmark tests

To evaluate the performance of the `parallelproj` projectors using the three computation modes described above, we implemented a series of benchmarking tests. All tests are related to a PET image reconstruction task and used the geometry and properties of a state-of-the-art GE Discovery MI TOF PET/CT scanner [30] with 20 cm axial FOV. This scanner consists of 36 detector “rings”, where each “ring” has a radius of 380 mm and consists of 34 modules containing 16 detectors each such that there are $16 \times 34 \times 36 = 19584$ detectors in total. A non-TOF emission sinogram for this scanner in span 1 has 415 radial elements, 272 views, and 1292 planes, meaning that for a full non-TOF sinogram projection, $415 \times 272 \times 1292 = 146e6$ line integrals have to be evaluated. For TOF data, each line of response (LOR) is subdivided into 29 TOF bins using a TOF bin width of 169 ps. The reported TOF resolution of the scanner is 375 ps FWHM [30]. In the TOF projectors of `parallelproj`, the Gaussian TOF kernel is truncated beyond ± 3 standard deviations.

To evaluate the performance of `parallelproj` for projections in sinogram mode, we measured the time needed for a forward and back projection of a span 1 subset sinogram containing 8 equally spaced views in non-TOF and TOF mode. This is equivalent to the projection work required for an OSEM subset update using 34 subsets in total, a setting that is used in many clinical reconstructions. Since it is known that the in-memory data order severely affects the computation time, especially on CUDA devices, we varied the order of the spatial axis of the sinogram, as well as the orientation of the symmetry axis of the scanner. E.g. in the sinogram order mode “PVR”, the radial direction increased the fastest and the plane direction increased the slowest in memory. For the sinogram order mode “VRP”, the plane direction increased the fastest and the view direction the slowest. By varying the orientation of the scanner symmetry axis, we could test the impact of different image volume memory layouts. For example, the symmetry axis mode “2” meant that the image volume memory increased the fastest in the axial direction of the scanner, while “0” or “1” meant that one of the transaxial directions increased the fastest.

In addition to the sinogram projection tests, we also evaluated the performance of `parallelproj` for non-TOF and TOF projections in listmode as a function of

the number of acquired listmode events. Instead of randomly generating the event coordinates, listmode events from an acquisition of a NEMA image quality phantom were used, which guaranteed a more realistic event distribution. In contrast to the projections in sinogram mode, where the ray directions and memory access are somehow ordered, they are random for unsorted listmode data. Similarly to the sinogram tests, the symmetry axis of the scanner was also varied. For all sinogram and listmode projection benchmarks, the coordinates of all LOR start and endpoints were precalculated such that the overhead of calculating the LOR coordinates was not included in these tests. All benchmarks were repeated 10 times and the mean and standard deviation of the results were calculated and visualized.

Finally, we also measured the time needed for a complete listmode OSEM iteration using 34 subsets as a function of the number of listmode events in the NEMA acquisition. In contrast to the projection benchmarks, the LOR start and end points were not precalculated. Instead, they were generated by indexing a lookup table stored in CPU or GPU memory containing all detector coordinates using the transaxial and axial detector numbers provided in the original listmode file.

All tests used an image of size (215,215,71), an isotropic voxel size of 2.78 mm, and were performed on a workstation including an AMD Ryzen Threadripper PRO 3955WX 16 core 32 thread CPU with 256 GB RAM, and an NVIDIA GeForce RTX 3090 GPU with 24 GB RAM on Ubuntu 20.04 LTS using CUDA v11.2 and `parallelproj` v1.2.9. The scanner geometry, as well as the list mode OSEM algorithm, was implemented in a minimal proof-of-concept Python package available at <https://github.com/gschramm/pyparallelproj>. For the CPU and hybrid CPU/GPU mode, Python’s `ctypes` module is used to project numpy arrays stored in CPU (host) memory using a minimal interface to the low level projection functions defined in `libparallelproj_c` and `libparallelproj_cuda`. In GPU mode, the CUDA projection kernels were just in time compiled and directly executed on cupy GPU arrays. Due to the interoperability between numpy and cupy the same high-level listmode OSEM implementation could be used for both modes. Note that in the latter, all operations needed for the OSEM update were executed directly on the cupy GPU arrays, eliminating any memory transfer between the host and the GPU during OSEM updates. In all listmode OSEM reconstructions, a shift-invariant image-based resolution model was used, including a Gaussian kernel of 4.5 mm FWHM.

3 Results

Figures 2 and 3 show the results of the sinogram benchmarks in non-TOF and TOF mode, respectively. In non-TOF mode, the best results in terms of the summed time needed for the forward and back projection of one subset sinogram were (compute mode, sinogram order

mode, scanner symmetry axis): 1.50 s for (CPU, PVR, 0), 0.053 s for (hybrid CPU / GPU, RVP, 2) and 0.025 s for (GPU, RVP, 2), meaning that the pure GPU mode was approximately 60x faster than the CPU mode and 2.1x faster than the hybrid mode. In TOF mode, the corresponding results were: 8.99 s for (CPU, PVR, 0), 0.277 s for (hybrid CPU/GPU, RVP, 2), and 0.189 s for (GPU, RVP, 2), which means that the pure GPU mode was approximately 48x faster than the CPU mode and 1.5x faster than the hybrid mode. As expected, especially for the back projections where atomic operations are used, the memory order in the sinogram as well as in the image has a substantial impact on the results. The ratios between the best and worst results for the combined projection times in terms of sinogram order and symmetry axis (non-TOF, TOF mode) were: (2.5, 1.6) in the CPU mode, (4.2, 3.0) in the hybrid mode, and (8.0, 4.0) in the GPU mode.

Figures 4 and 5 show the results of the listmode benchmarks in non-TOF and TOF mode, respectively. For 40e6 events, the best results in terms of time needed for the forward and back projection (non-TOF, TOF) were: (34.8, s, 10.6, s) in CPU mode, (4.09 s, 0.75 s) in hybrid mode and (3.91 s, 0.58 s) in GPU mode. For 1.25e6 events, the best results in terms of time needed for the forward and back projection (non-TOF, TOF) were: (1.08 s, 0.34 s) in CPU mode, (0.11 s, 0.029 s) in hybrid mode, and (0.1 s, 0.018 s) in GPU mode. In non-TOF mode, the pure GPU mode was approximately 10x faster than the CPU mode and 1.1x faster than the hybrid mode. In TOF mode, the pure GPU mode was approximately 20x faster than the CPU mode and 1.6x faster than the hybrid mode. In contrast to the sinogram benchmark results, the impact of the scanner symmetry axis direction was small. In the CPU and GPU mode, the increase in projection time as a function of the number of list-mode events was almost perfectly linear. In hybrid mode at low number of events, the scaling was not linear due to the overhead caused by the time needed for memory transfer.

Figure 6 shows the results for the timing of a complete TOF listmode OSEM iteration, including 34 subset updates, as well as a reconstruction of the NEMA image quality phantom data set using 40e6 total prompt events. The best results for (40e6, 1.25e6) events were: (18.47 s, 3.77 s) in CPU mode, (8.48 s, 3.39 s) in hybrid mode, and (0.63 s, 0.065 s) in GPU mode which means that for 40e6 events the pure GPU mode was approximately 29x faster than the CPU mode and 13.4x faster than the hybrid mode.

4 Discussion

All results shown in our article demonstrate once more that parallel computation of forward and back projections using a state-of-the-art GPU is substantially faster

compared to parallelization using OpenMP on a state-of-the-art multicore CPU system. Certainly, the achievable GPU acceleration factor strongly depends on the computational problem itself (e.g. sinogram or listmode reconstruction) and the problem size. In our non-TOF and TOF sinogram and listmode benchmark tests, we observed GPU acceleration factors between 10 and 60.

One important aspect that emerged from our sinogram benchmark tests - where the projection data and memory access is ordered - is the fact that the projection times varied substantially when using different memory layouts (up to a factor of 8 in the GPU mode). This can be understood by taking into account that the amount of race conditions that are created during the back projection within a thread block heavily depends on the order and possible intersections of rays to be projected within that block. Note that in pure GPU mode, the time needed for sinogram forward projections also varied substantially across the different memory layouts, which is probably due to the way image memory is accessed and cached on CUDA GPUs.

Another interesting observation is the fact that in all compute modes the time needed to calculate TOF sinogram projections was much longer than the times needed to calculate non-TOF sinogram projections, whereas the situation was reversed in listmode. For TOF sinogram projections, more floating point operations have to be computed compared to non-TOF sinogram projections due to the evaluations of the TOF kernels between the contributing voxels and a number of TOF bins. In listmode, however, the computational work needed to project a TOF event is much lower compared to projecting a non-TOF event. This is the case because a TOF listmode event detected in a specific TOF bin is only affected by a few voxels along the complete LOR in the image, where the number of affected voxels is inversely proportional to the TOF resolution of the scanner. That in turn means that with scanner TOF resolutions becoming better and better, the gap between the TOF projection times in sinogram and listmode will become bigger and bigger, strongly favoring listmode processing. According to our experience, projection times in listmode are already much faster for most standard clinical acquisitions (except for very long static brain scans with high affinity tracers) on current PET systems with TOF resolutions between 250-400 ps.² Extrapolating the timing results of one complete OSEM listmode iteration of an acquisition with 40e6 counts in Figure 6, clinical listmode OSEM reconstructions of a single bed position of a standard static FDG whole-body acquisition using PET scanner with 20-25 cm axial FOV seem to be possible in a couple of seconds and could even be faster than the acquisition time.³

A somewhat unexpected result was the fact that the gap in the TOF projection times between hybrid CPU/GPU and pure GPU mode was much bigger when timing

²An alternative way to further accelerate sinogram-based reconstructions is the use of dedicated sinogram rebinning techniques.

³This is obviously only true if all other necessary corrections, such as scatter estimation, can be performed very quickly as well. For PET scanners with a very long axial field of view (much higher sensitivity), the reconstruction times could be substantially longer.

the execution of a complete listmode OSEM iteration compared to the pure projection benchmark test when reconstruction 40e6 counts (approximately a factor of 13 vs a factor of 1.6, respectively). After detailed profiling of a listmode OSEM iteration in hybrid mode, it became obvious that the total time spent for the 34 subset listmode forward and back projections (ca. 1.2 s) was short compared to the time needed to calculate all other operations necessary for the OSEM update. Profiling revealed that calculating the LOR start and end coordinates using the lookup table approach took approximately 3.5 s and that calculating all 68 Gaussian convolutions needed for image-based resolution modeling took approximately 2.3 s. Keep in mind that those operations were performed on the CPU in hybrid compute mode. While the overhead due to the lookup of the LOR start and end coordinates can be completely eliminated by precalculating those coordinates, reducing the overhead caused by the CPU-based Gaussian convolution is more complicated, but probably possible as well, which would bring the reconstruction time gap closer to the gap observed in the pure projection benchmarks. An interesting lesson to be learned is that once very fast GPU-based projectors are used, it should always be double-checked whether other computational steps of any algorithm become new bottlenecks.

An important limitation of our study is the fact that we only implemented and benchmarked Joseph's projection method. Compared to other methods such as the distance-driven method, multiray models, or tube-of-response models, Joseph's method is inherently faster. Consequently, projection times are expected to be somewhat slower for more advanced projectors, but a detailed investigation of more advanced projectors is beyond the scope of this work and left for future research.⁴ Note, however, that according to our experience, combining Joseph's method with an image-based and / or sinogram-based resolution model produces high-quality PET reconstructions.

Without a doubt, it is possible to further optimize the implementation of the `parallelproj` projectors, especially the CUDA implementation. As an example, we have decided not to use CUDA's texture memory, which could substantially accelerate the image interpolations needed in the Joseph forward projections, or be also used to interpolate TOF kernel values based on a 1D lookup table. The main reason for not using texture memory is the fact that it would only accelerate the forward projections since writing into texture memory is not possible and because reconstruction times are usually dominated by the back projections. Another way to further improve the listmode projection times is to pre-sort the listmode events to minimize race conditions during back projection, as e.g. shown in [9].

⁴Since `parallelproj` is an open-source project, contributions of or discussions on more advanced projectors from the reconstruction community are more than welcome.

5 Conclusion

`parallelproj` is an open-source, and easy accessible research framework for efficient calculation of non-TOF and TOF projections in sinogram or listmode on multiple CPUs or state-of-the-art CUDA GPUs. Conventional and advanced research reconstructions (including deep learning) can be substantially accelerated by using the hybrid and pure GPU compute modes of this framework.

References

- [1] X. Zhang, J. Zhou, S. R. Cherry, R. D. Badawi, and J. Qi, "Quantitative image reconstruction for total-body pet imaging using the 2-meter long explorer scanner," *Physics in Medicine and Biology*, vol. 62, no. 6, p. 2465, 2017. DOI: [10.1088/1361-6560/aa5e46](https://doi.org/10.1088/1361-6560/aa5e46).
- [2] F. Lamare, A. Bousse, K. Thielemans, C. Liu, T. Merlin, H. Fayad, and D. Visvikis, "Pet respiratory motion correction: Quo vadis?" *Physics in Medicine and Biology*, vol. 67, no. 3, 03TR02, 2022. DOI: [10.1088/1361-6560/ac43fc](https://doi.org/10.1088/1361-6560/ac43fc).
- [3] G. Wang, J. C. Ye, K. Mueller, and J. A. Fessler, "Image reconstruction is a new frontier of machine learning," *IEEE Transactions on Medical Imaging*, vol. 37, no. 2, pp. 1–14, 2018. DOI: [10.1109/TMI.2018.2833635](https://doi.org/10.1109/TMI.2018.2833635).
- [4] G. Wang, J. C. Ye, and B. De Man, "Deep learning for tomographic image reconstruction," *Nature Machine Intelligence*, vol. 2, no. 12, pp. 737–748, 2020, Publisher: Springer US. DOI: [10.1038/s42256-020-00273-z](https://doi.org/10.1038/s42256-020-00273-z).
- [5] A. J. Reader, G. Corda, A. Mehranian, C. d. Costa-Luis, S. Ellis, and J. A. Schnabel, "Deep learning for pet image reconstruction," *IEEE Transactions on Radiation and Plasma Medical Sciences*, vol. 5, no. 1, pp. 1–25, 2021. DOI: [10.1109/TRPMS.2020.3014786](https://doi.org/10.1109/TRPMS.2020.3014786).
- [6] G. Pratz, G. Chinn, F. Habte, P. Olcott, and C. Levin, "Fully 3-d list-mode OSEM accelerated by graphics processing units," in *2006 IEEE Nuclear Science Symposium Conference Record*, ISSN: 1082-3654, vol. 4, Oct. 2006, pp. 2196–2202. DOI: [10.1109/NSSMIC.2006.354350](https://doi.org/10.1109/NSSMIC.2006.354350).
- [7] G. Pratz, G. Chinn, P. D. Olcott, and C. S. Levin, "Fast, accurate and shift-varying line projections for iterative reconstruction using the GPU," *IEEE Transactions on Medical Imaging*, vol. 28, no. 3, pp. 435–445, Mar. 2009, Conference Name: IEEE Transactions on Medical Imaging. DOI: [10.1109/TMI.2008.2006518](https://doi.org/10.1109/TMI.2008.2006518).
- [8] W. C. Barker, S. Thada, and W. Dieckmann, "A GPU-accelerated implementation of the MOLAR PET reconstruction package," in *2009 IEEE Nuclear Science Symposium Conference Record (NSS/MIC)*, ISSN: 1082-3654, Oct. 2009, pp. 4114–4119. DOI: [10.1109/NSSMIC.2009.5402353](https://doi.org/10.1109/NSSMIC.2009.5402353).
- [9] J.-y. Cui, G. Pratz, S. Prevrhal, and C. S. Levin, "Fully 3d list-mode time-of-flight PET image reconstruction on GPUs using CUDA," *Medical Physics*, vol. 38, no. 12, pp. 6775–6786, 2011, eprint: <https://onlinelibrary.wiley.com/doi/pdf/10.1118/1.3661998>. DOI: [10.1118/1.3661998](https://doi.org/10.1118/1.3661998).
- [10] J. L. Herraiz, S. España, J. Cal-González, J. J. Vaquero, M. Desco, and J. M. Udías, "Fully 3d GPU PET reconstruction," *Nuclear Instruments and Methods in Physics Research Section A: Accelerators, Spectrometers, Detectors and Associated Equipment*, NIMA_4th International Conference on Imaging techniques in Subatomic Physics, Astrophysics, Medicine, Biology and Industry, vol. 648, S169–S171, Aug. 21, 2011. DOI: [10.1016/j.nima.2010.12.043](https://doi.org/10.1016/j.nima.2010.12.043).

- [11] J. L. Herraiz, S. España, R. Cabido, A. S. Montemayor, M. Desco, J. J. Vaquero, and J. M. Udías, "GPU-based fast iterative reconstruction of fully 3-d PET sinograms," *IEEE Transactions on Nuclear Science*, vol. 58, no. 5, pp. 2257–2263, Oct. 2011, Conference Name: IEEE Transactions on Nuclear Science. DOI: [10.1109/TNS.2011.2158113](https://doi.org/10.1109/TNS.2011.2158113).
- [12] K. S. Kim and J. C. Ye, "Fully 3d iterative scatter-corrected OSEM for HRRT PET using a GPU," *Physics in Medicine and Biology*, vol. 56, no. 15, p. 4991, Jul. 2011. DOI: [10.1088/0031-9155/56/15/021](https://doi.org/10.1088/0031-9155/56/15/021).
- [13] J. Zhou and J. Qi, "Fast and efficient fully 3d PET image reconstruction using sparse system matrix factorization with GPU acceleration," *Physics in Medicine and Biology*, vol. 56, no. 20, p. 6739, Oct. 2011. DOI: [10.1088/0031-9155/56/20/015](https://doi.org/10.1088/0031-9155/56/20/015).
- [14] C.-Y. Chou, Y. Dong, Y. Hung, Y.-J. Kao, W. Wang, C.-M. Kao, and C.-T. Chen, "Accelerating image reconstruction in dual-head PET system by GPU and symmetry properties," *PLOS ONE*, vol. 7, no. 12, e50540, Dec. 26, 2012, Publisher: Public Library of Science. DOI: [10.1371/journal.pone.0050540](https://doi.org/10.1371/journal.pone.0050540).
- [15] S. Kinouchi, T. Yamaya, E. Yoshida, H. Tashima, H. Kudo, H. Haneishi, and M. Suga, "GPU-based PET image reconstruction using an accurate geometrical system model," *IEEE Transactions on Nuclear Science*, vol. 59, no. 5, pp. 1977–1983, Oct. 2012, Conference Name: IEEE Transactions on Nuclear Science. DOI: [10.1109/TNS.2012.2201953](https://doi.org/10.1109/TNS.2012.2201953).
- [16] J. Cui, G. Pratz, B. Meng, and C. S. Levin, "Distributed MLEM: An iterative tomographic image reconstruction algorithm for distributed memory architectures," *IEEE Transactions on Medical Imaging*, vol. 32, no. 5, pp. 957–967, May 2013, Conference Name: IEEE Transactions on Medical Imaging. DOI: [10.1109/TMI.2013.2252913](https://doi.org/10.1109/TMI.2013.2252913).
- [17] S. Ha, S. Matej, M. Ispiryan, and K. Mueller, "GPU-accelerated forward and back-projections with spatially varying kernels for 3d DIRECT TOF PET reconstruction," *IEEE Transactions on Nuclear Science*, vol. 60, no. 1, pp. 166–173, Feb. 2013, Conference Name: IEEE Transactions on Nuclear Science. DOI: [10.1109/TNS.2012.2233754](https://doi.org/10.1109/TNS.2012.2233754).
- [18] P. J. Markiewicz, K. Thielemans, M. J. Ehrhardt, J. Jiao, N. Burgos, D. Atkinson, S. R. Arridge, B. F. Hutton, and S. Ourselin, "High throughput CUDA implementation of accurate geometric modelling for iterative reconstruction of PET data," in *2014 IEEE Nuclear Science Symposium and Medical Imaging Conference (NSS/MIC)*, Nov. 2014, pp. 1–4. DOI: [10.1109/NSSMIC.2014.7430963](https://doi.org/10.1109/NSSMIC.2014.7430963).
- [19] J. Zhou and J. Qi, "Efficient fully 3d list-mode TOF PET image reconstruction using a factorized system matrix with an image domain resolution model," *Physics in Medicine and Biology*, vol. 59, no. 3, p. 541, Jan. 2014, Publisher: IOP Publishing. DOI: [10.1088/0031-9155/59/3/541](https://doi.org/10.1088/0031-9155/59/3/541).
- [20] M. A. Nassiri, J.-F. Carrier, and P. Després, "Fast GPU-based computation of spatial multigrid multiframe LMEM for PET," *Medical and Biological Engineering and Computing*, vol. 53, no. 9, pp. 791–803, Sep. 1, 2015. DOI: [10.1007/s11517-015-1284-9](https://doi.org/10.1007/s11517-015-1284-9).
- [21] T. Zeng, J. Gao, D. Gao, Z. Kuang, Z. Sang, X. Wang, L. Hu, Q. Chen, X. Chu, D. Liang, X. Liu, Y. Yang, H. Zheng, and Z. Hu, "A GPU-accelerated fully 3d OSEM image reconstruction for a high-resolution small animal PET scanner using dual-ended readout detectors," *Physics in Medicine and Biology*, vol. 65, no. 24, p. 245 007, Dec. 2020, Publisher: IOP Publishing. DOI: [10.1088/1361-6560/aba6f9](https://doi.org/10.1088/1361-6560/aba6f9).
- [22] A. Eklund, P. Dufort, D. Forsberg, and S. M. LaConte, "Medical image processing on the GPU – past, present and future," *Medical Image Analysis*, vol. 17, no. 8, pp. 1073–1094, Dec. 1, 2013. DOI: [10.1016/j.media.2013.05.008](https://doi.org/10.1016/j.media.2013.05.008).
- [23] P. Depres and X. Jia, "A review of GPU-based medical image reconstruction | elsevier enhanced reader," vol. 42, pp. 76–92, 2017. DOI: [10.1016/j.ejomp.2017.07.024](https://doi.org/10.1016/j.ejomp.2017.07.024).
- [24] R. Okuta, Y. Unno, D. Nishino, S. Hido, and C. Loomis, "Cupy: A numpy-compatible library for nvidia gpu calculations," in *Proceedings of Workshop on Machine Learning Systems (LearningSys) in The Thirty-first Annual Conference on Neural Information Processing Systems (NIPS)*, 2017.
- [25] A. Paszke, S. Gross, F. Massa, A. Lerer, J. Bradbury, G. Chanan, T. Killeen, Z. Lin, N. Gimeshine, L. Antiga, A. Desmaison, A. Kopf, E. Yang, Z. DeVito, M. Raison, A. Tejani, S. Chilamkurthy, B. Steiner, L. Fang, J. Bai, and S. Chintala, "Pytorch: An imperative style, high-performance deep learning library," in *Advances in Neural Information Processing Systems*, H. Wallach, H. Larochelle, A. Beygelzimer, F. d'Alché-Buc, E. Fox, and R. Garnett, Eds., vol. 32, Curran Associates, Inc., 2019.
- [26] R. L. Siddon, "Fast calculation of the exact radiological path for a three-dimensional CT array," *Medical Physics*, vol. 12, no. 2, pp. 252–255, 1985, eprint: <https://onlinelibrary.wiley.com/doi/pdf/10.1118/1.595715>. DOI: [10.1118/1.595715](https://doi.org/10.1118/1.595715).
- [27] B. De Man and S. Basu, "Distance-driven projection and back-projection in three dimensions," *Physics in medicine and biology*, vol. 49, no. 11, pp. 2463–2475, 2004, ISBN: 0-7803-7636-6. DOI: [10.1109/NSSMIC.2002.1239600](https://doi.org/10.1109/NSSMIC.2002.1239600).
- [28] P. M. Joseph, "An improved algorithm for reprojecting rays through pixel images," *IEEE Transactions on Medical Imaging*, vol. 1, no. 3, pp. 192–196, 1982. DOI: [10.1109/TMI.1982.4307572](https://doi.org/10.1109/TMI.1982.4307572).
- [29] L. Dagum and R. Menon, "Openmp: An industry standard api for shared-memory programming," *IEEE Computational Science and Engineering*, vol. 5, no. 1, pp. 46–55, 1998. DOI: [10.1109/99.660313](https://doi.org/10.1109/99.660313).
- [30] D. F. Hsu, E. Ilan, W. T. Peterson, J. Uribe, M. Lubberink, and C. S. Levin, "Studies of a next-generation silicon-photomultiplier-based time-of-flight PET/CT system," *Journal of Nuclear Medicine*, vol. 58, no. 9, pp. 1511–1518, 2017. DOI: [10.2967/jnumed.117.189514](https://doi.org/10.2967/jnumed.117.189514).

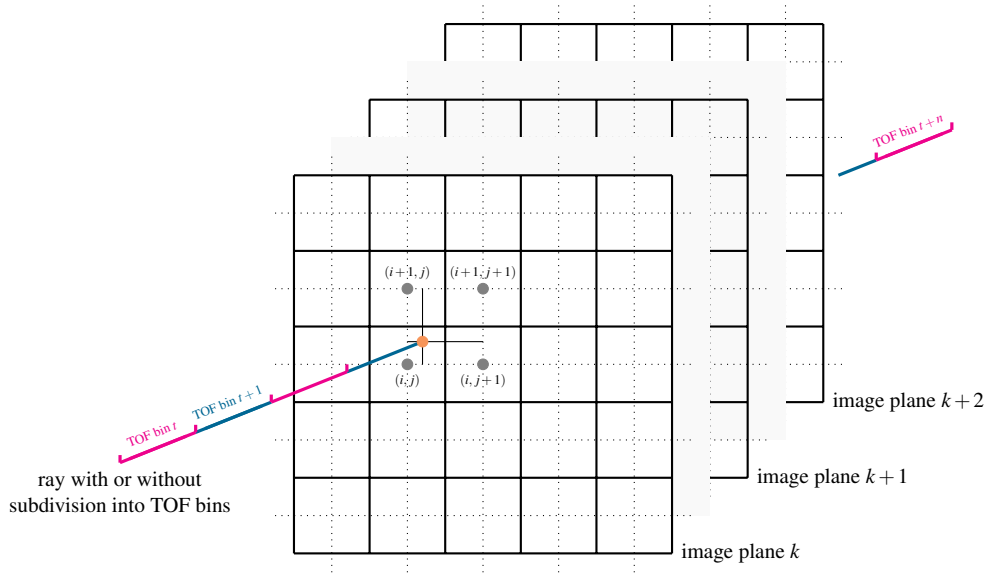


Figure 1: Illustration of Joseph's method for projecting rays through voxel images. In a ray-driven approach the image volume is traversed plane by plane along a principal direction. At every plane, the intersection point between the ray and image plane is calculated (orange dot). The contribution of the four nearest voxels (gray dots) to the line integral is modeled using bi-linear interpolation weights. The method can also be easily extended to compute TOF-weighted projections using a subdivision of the ray into TOF bins and by evaluation of a TOF kernel. See text and [28] for more details. Figure not drawn to scale.

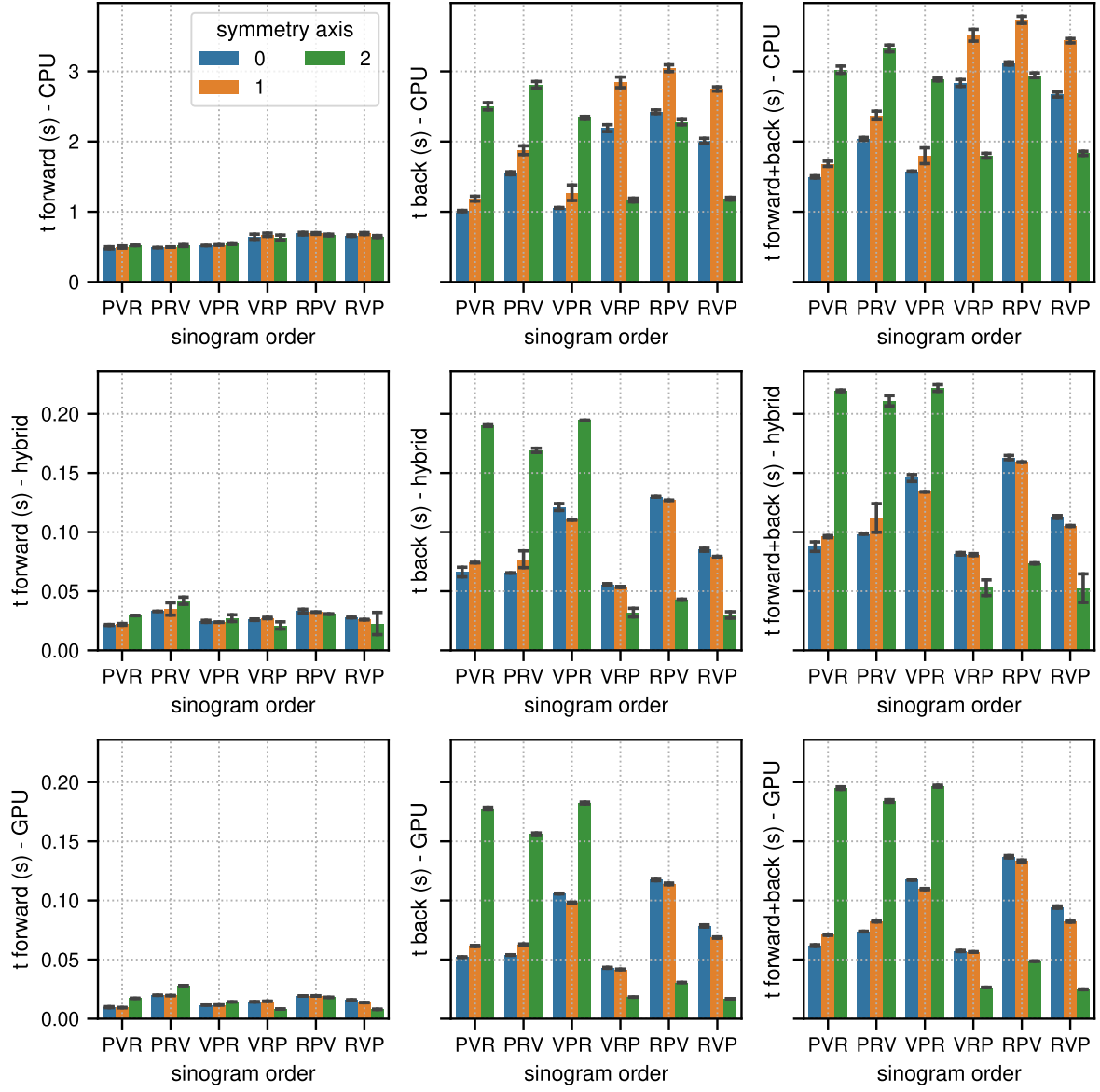


Figure 2: Results of the non-TOF sinogram benchmark tests. The non-TOF subset sinogram contained 415 radial elements, 8 views and 1292 planes (1 out of 34 subsets). The image used in these tests contained (215,215,71) voxels with an isotropic voxel size of 2.78 mm. The mean and the standard deviation estimated from 10 runs are represented by the colored bars and the black error bars, respectively. Note the different limits on the y axes.

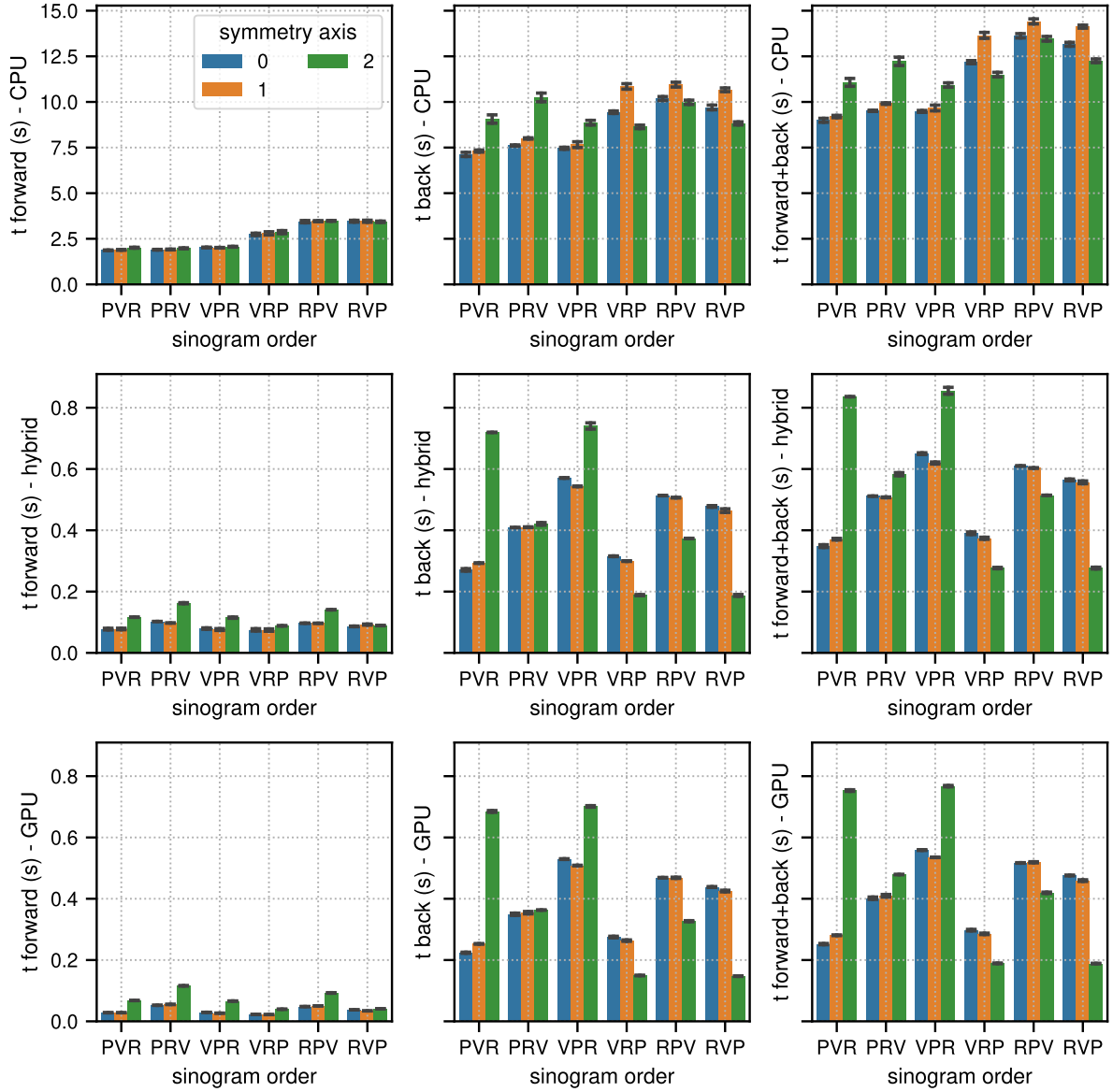


Figure 3: Results of the TOF sinogram benchmark tests. The TOF subset sinogram contained 415 radial elements, 8 views, 1292 planes and 29 TOF bins with a width of 169 ps. The modeled TOF resolution was 375 ps. The image used in these tests contained (215,215,71) voxels with an isotropic voxel size of 2.78 mm. The mean and the standard deviation estimated from 10 runs are represented by the colored bars and the black error bars, respectively. Note the different limits on the y axes.

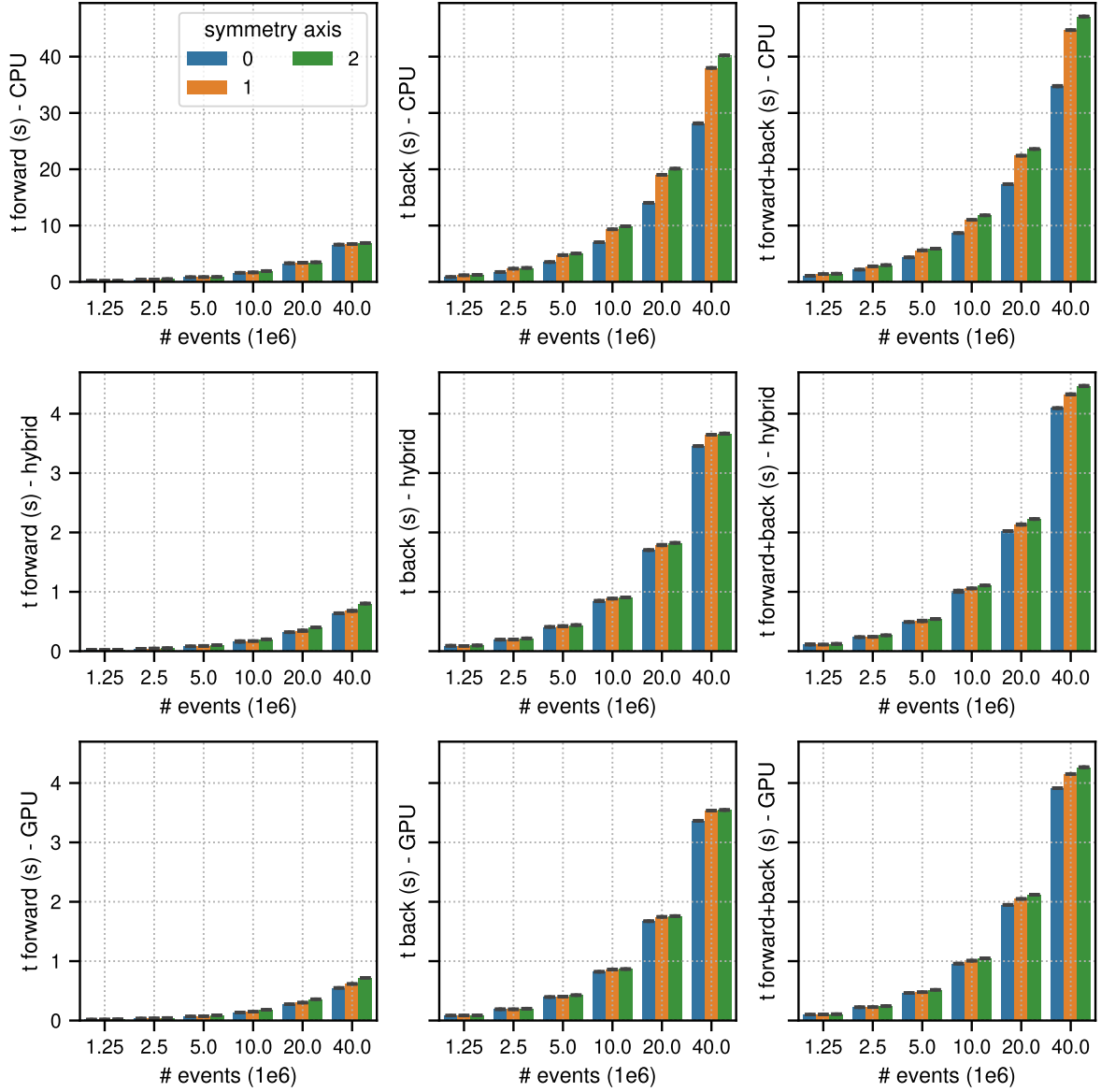


Figure 4: Results of the non-TOF listmode benchmark tests for different number of listmode events. The image used in these tests contained (215,215,71) voxels with an isotropic voxel size of 2.78 mm. The mean and the standard deviation estimated from 10 runs are represented by the colored bars and the black error bars, respectively. Note the different limits on the y axes and that the x-axis scale is non-linear.

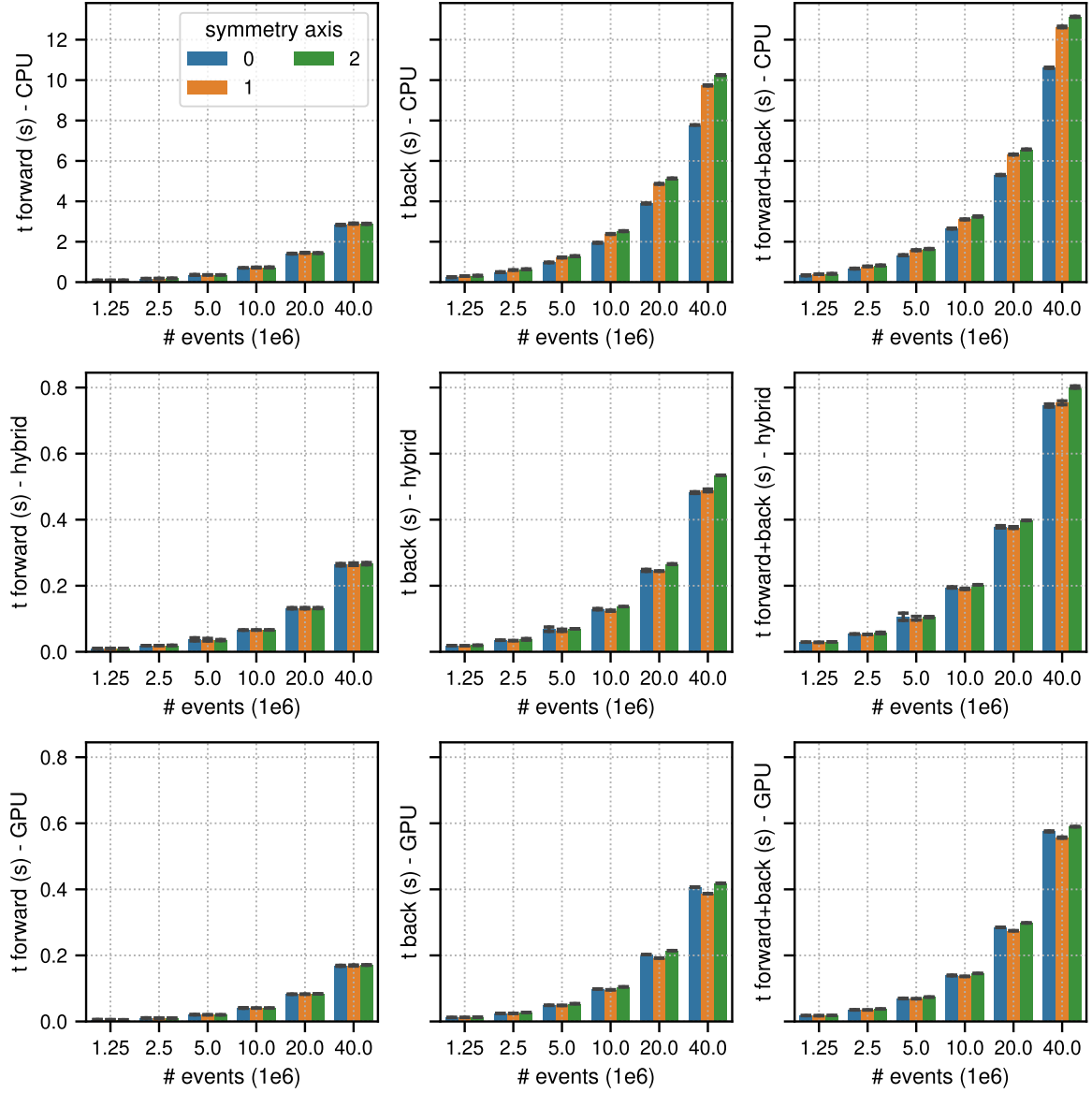


Figure 5: Results of the TOF listmode benchmark tests for different number of listmode events. The image used in these tests contained (215,215,71) voxels with an isotropic voxel size of 2.78 mm. The mean and the standard deviation estimated from 10 runs are represented by the colored bars and the black error bars, respectively. Note the different limits on the y axes and that the x-axis scale is non-linear.

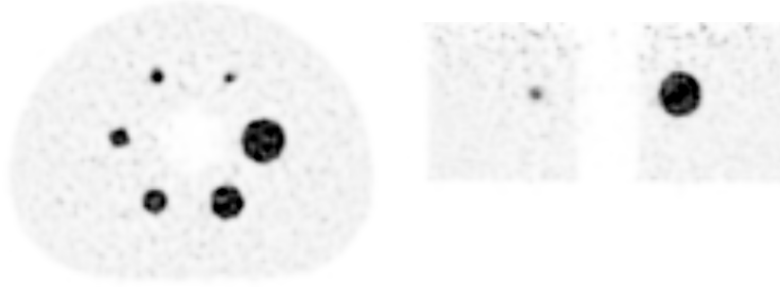
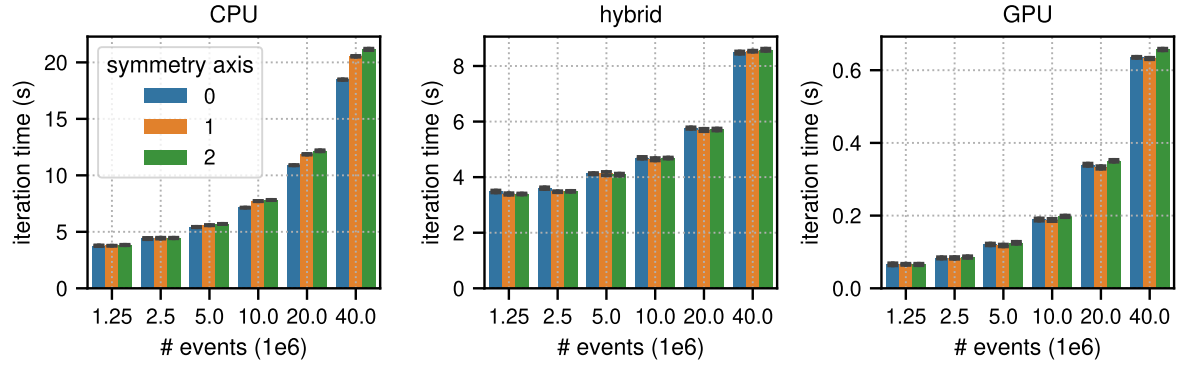


Figure 6: (top) Results for the timing of a complete LM OSEM iteration including 34 subset updates for the NEMA image quality phantom acquisition. The image used in these tests contained (215,215,71) voxels with an isotropic voxel size of 2.78 mm. The mean and the standard deviation estimated from 6 iterations are represented by the colored bars and the black error bars, respectively. Note the different limits on the y axes and that the x-axis scale is non-linear. (bottom) Transaxial and coronal slice of a listmode OSEM reconstruction of the NEMA image quality phantom with 40e6 events after 6 iterations with 34 subsets using a standard Gaussian post filter of 4 mm FWHM. Note that for better visibility, the reconstructed image was cropped to the center portion of the transaxial FOV.